

## The Flow Structures of a Transversely Rotating Sphere at High Rotation Rates

J. Dobson<sup>1,2</sup>, A. Ooi<sup>1</sup> and E. K. W. Poon<sup>1</sup>

<sup>1</sup>Department of Mechanical Engineering  
 University of Melbourne, Parkville, Victoria 3010, Australia

<sup>2</sup>Department of Mechanical Engineering  
 Imperial College of Science Technology and Medicine, London SW7 2A2, United Kingdom

### Abstract

The near wake flow structures of a steady, transversely rotating sphere at Reynolds number,  $Re = 300$ , and high rotational rates,  $\Omega^* \in [1.50, 3.00]$ , where  $\Omega^*$  is the maximum sphere surface velocity normalised by the free stream velocity, are numerically investigated. Within this range of rotational rates, the near wake flow structures undergo multiple flow transitions. The near wake flow structures lose planar symmetry for the first time for  $\Omega^* = 2.00$  to  $2.25$ , but planar symmetry is restored for  $\Omega^* = 2.50$  to  $2.75$ . At  $\Omega^* = 3.00$ , the high sphere surface velocity leads to spiralling motions along the rotation axis. These spiralling motions react with the uniform free stream that leading to small scale energetic flow structures on the advancing side of the sphere (where the sphere surface velocity is opposite to the free stream velocity). Consequently, the flow structures depart from planar symmetry. The presence of small scale vortices dramatically increases the oscillating frequency of the hydrodynamic forces acting on the sphere. The increase in sphere rotation rate,  $\Omega^*$ , also results in better pressure recovery on the lee side of the sphere. As a result, the time-averaged drag coefficient decreases monotonically for  $1.50 < \Omega^* \leq 3.00$ .

### Introduction

For many decades researchers have sought to understand the flow structures which occur when a fluid passes over a uniformly rotating solid sphere. Sphere rotation was shown to have an impact on the forces the sphere experiences as well as enhancing turbulence in the surrounding flow [1]. This information is of interest because it provides a basic model for the forces which are present in particle laden flows. Rubinow and Keller [12], using the Stokes and Oseen expansion of the Navier–Stokes equations, provided one of the early contributions of lift force,  $F_L$ , in the limit of very low Reynolds number ( $Re = \rho U_\infty d / \mu \leq 0.1$ ) and low rotation rate ( $\Omega^* = \omega d / 2U_\infty \leq 0.10$ ), where  $\rho$  and  $\mu$  respectively refer to fluid density and dynamic viscosity,  $U_\infty$  stands for free stream velocity,  $d$  is the sphere diameter and  $\omega$  represents the angular velocity of the sphere. Above this range of Reynolds number and rotation rate, numerous experimental studies had been carried out [2, 8, 10, 13, 14]. An excellent review of the literature by Loth [7] has identified the global trends of lift coefficients,  $C_L$ , across different conditions.

The use of numerical simulations at the beginning of 90s has provided an insight into the flow structures of a rotating sphere which have been lacking from most of the experimental studies. However, apart from the numerical study carried out by You *et al.* [15] at  $Re < 68.4$  and  $\Omega^* < 5$ , numerical studies at moderate Reynolds numbers ( $Re \leq 300$ ) are limited to low rotational rate ( $\Omega^* \leq 1.2$ ) only [3, 6, 11]. The aim of this study is to expand the understanding of the flow to conditions at higher rotation rates, in the range of  $\Omega^* = 1.50$ – $3.00$ .

### Problem Definition and Solution Procedures

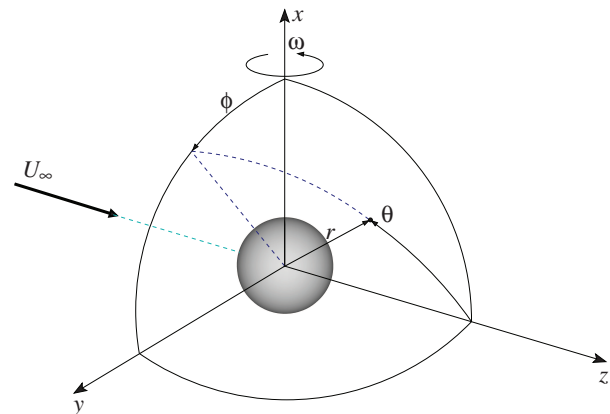


Figure 1: The spherical and the Cartesian coordinate systems. The free stream flow is aligned with the  $z$ -axis and sphere is rotating in the  $x$ -direction.

Figure 1 presents the basic geometry of the problem where a solid sphere is shown at the origin of the spherical coordinate system  $(r, \theta, \phi)$ . The free stream flow is aligned in the  $z$ -direction and the sphere is constrained to rotate in the  $x$ -direction. The fluid motion of a transversely rotating sphere is described by the incompressible Navier–Stokes equations,

$$\frac{d\vec{u}}{dt} + \vec{u} \cdot \nabla \vec{u} = -\nabla P + \frac{1}{Re} \nabla^2 \vec{u}, \quad (1)$$

$$\nabla \cdot \vec{u} = 0. \quad (2)$$

Equations (1) and (2) are solved using a well-developed Fourier–Chebyshev collocation method [3, 11] in a spatial domain being described in spherical coordinates. The numbers of collocation points in each direction are  $(n_r, n_\theta, n_\phi) = (121, 100, 64)$ . To improve resolution near the boundary layer, the collocation points are clustered towards the sphere surface in the  $r$ -direction, and near the shoulder of the sphere in the  $\theta$ -direction where the flow separates and shear layer locates. The temporal resolution is chosen to be  $\Delta t^* = \Delta t U_\infty / d = 5 \times 10^{-4}$  [3]. A Dirichlet boundary condition  $\vec{u} = (0, 0, 1)$  is applied at the inlet, a Neumann boundary condition,  $\partial P / \partial n = 0$  at the outlet, and a no-slip and no penetration boundary condition at the sphere surface. The sphere surface velocity is prescribed by equation (2.5) of Giacobello *et al.* [3]. Details of the numerical algorithm and velocity boundary condition can be referred to Poon *et al.* [11].

### Features of the Flow Field

#### Classification of Flow Regimes

Figure 2 presents the summary of flow structures, identified using Jeong and Hussain [4]  $\lambda_2$  vortex identification method, for  $Re = 300$  and  $\Omega^* = 1.50$ – $3.00$ . The value of  $\lambda_2$  used in this

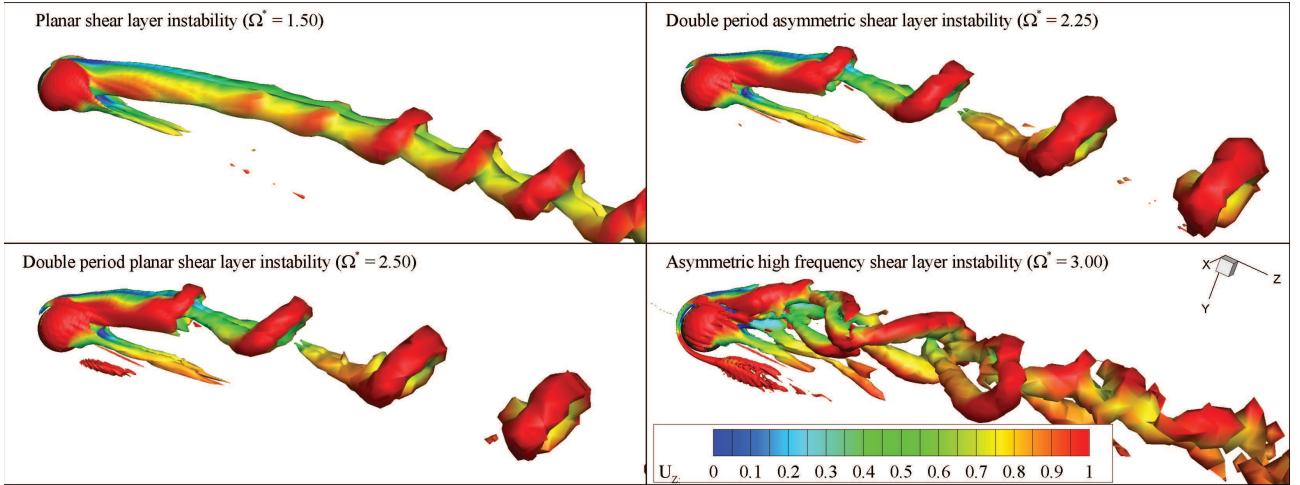


Figure 2: Representations of different flow regimes for a transversely rotating sphere at moderate  $Re$  and selected  $\Omega^*$ . The planar shear layer instability regime lies within  $\Omega^* = 0.80\text{--}1.50$ ; the double period planar shear layer instability regime is found at  $\Omega^* = 1.75, 2.50$  and  $2.75$ ; the double period asymmetric shear layer instability regime is in between  $\Omega^* = 2.00\text{--}2.25$  while the asymmetric high frequency shear layer instability at  $\Omega^* = 3.00$ .

study is  $\lambda_2 = -0.008$ . In general, between  $\Omega^* = 1.50\text{--}3.00$  the flow can be classified into four different regimes. One of these regimes, named ‘shear layer instability’ for  $\Omega^* = 1.50$ , shares behaviour with a previously identified classification by Giacobello *et al.* [3] and Kim [6] at  $Re = 300$ ,  $\Omega^* = 0.80\text{--}1.20$ , but the remaining three are to the authors knowledge new regimes as yet unreported in the literature. The flow from  $\Omega^* = 0.80\text{--}1.50$  is briefly discussed to provide context but the main focus is on the data produced in the present study.

For rotations in the range  $\Omega^* = 0.80$  through to  $1.50$ , the vortices are formed due to the shearing action of two flows with different bulk velocities. At the boundary between the two flow streams, a shearing motion occurs leading to a Kelvin–Helmholtz type instability. This shear force generates vorticity in the flow which is then enhanced as flow convect downstream. Under the present conditions this leads to the periodic formation and release of symmetric vortices at the end of the shear layer, which have a similar appearance to vortex shedding structures (see [5]) but are formed in a very different way. The frequency of the vortex formation due to shear layer instability is dependent on the velocity gradients between different streams and in this study, the frequency of vortices in this regime will be referred to as the ‘baseline’ frequency. The first data point in the present study at  $\Omega^* = 1.50$  lies within this regime.

At a rotation rate of  $\Omega^* = 1.75$  the flow is also characterised by the formation of vortices via the shear layer instability mechanism. However, the difference at this rotation rate is the fact that vortex formation occurs at a frequency which is approximately half the aforementioned ‘baseline’ frequency. As such, this flow has been termed ‘double period shear layer instability’. This drop in the frequency of rotation is thought to be caused by changes in the arrangement of shear layers at the rear of the sphere. The main impact of such a change in the vortices frequency is the fact that the oscillation frequency of the hydrodynamic forces will now be half of what it was previously. As with all previous regimes, the flow is however still planar.

In many ways the flow field at rotations of  $\Omega^* = 2.00$  and  $2.25$  is very similar to the flow at  $\Omega^* = 1.75$ . Due to shear layer instabilities in the flow there are regular vortices released from the shear layer, the frequency of which is a continuation from the previous regime. The difference now is that the flow is no

longer completely planar. Instead there is a small amount of out-of-plane motion in the flow as indicated by the  $(x, z)$ -plane view of the 3-dimensional streamlines pattern at  $\Omega^* = 2.00$  in figure 3. As such, this flow regime has been termed ‘double period asymmetric shear layer instability’.

Once the sphere rotation reaches  $\Omega^* = 2.50$  the flow has once more reverted to the ‘double period planar shear layer instabil-

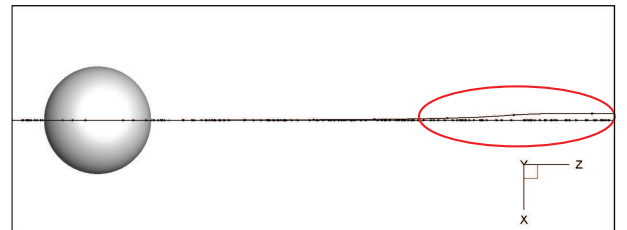


Figure 3:  $(x, z)$ -plane view of the 3-dimensional streamlines pattern at  $\Omega^* = 2.00$ . Red ellipse highlights the out-of-plane fluid motion in the  $x$ -direction.

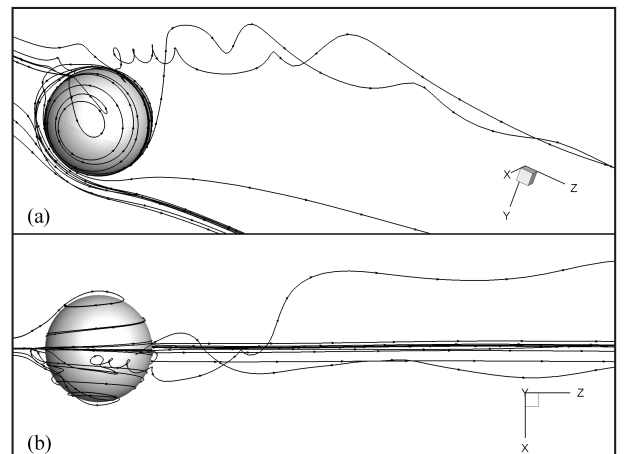


Figure 4: 3-dimensional streamlines pattern at  $\Omega^* = 3.00$ : (a) isometric view and (b)  $(x, z)$ -plane view.

ity regime' and this set of flow conditions persists up to a rotation of  $\Omega^* = 2.75$ . At a rotation of  $\Omega^* = 3.00$  there is a sharp change in the flow behaviour and a transition to what has been termed the 'asymmetric high frequency shear layer instability' regime occurs. At this rotation rate, the iso-surfaces of the flow structures not only become asymmetric, they also appear to be highly irregular in shape, unlike the asymmetric cases observed at  $\Omega^* = 2.00$  and 2.25. One of the primary reasons for the highly irregular flow structures at  $\Omega^* = 3.00$  can be attributed to the circulations appearing on shoulder of the sphere along the rotation axis as shown in figure 4. These circulations, which have not been observed for lower rotation rates, react with the upstream flow and results in small scale energetic flow on the advancing side (negative y-axis) of the sphere. The presence of the small scale energetic flow leads to a strong departure from planar symmetry and thus substantially increases  $C_{Lx}$ .

### Phase Behaviour

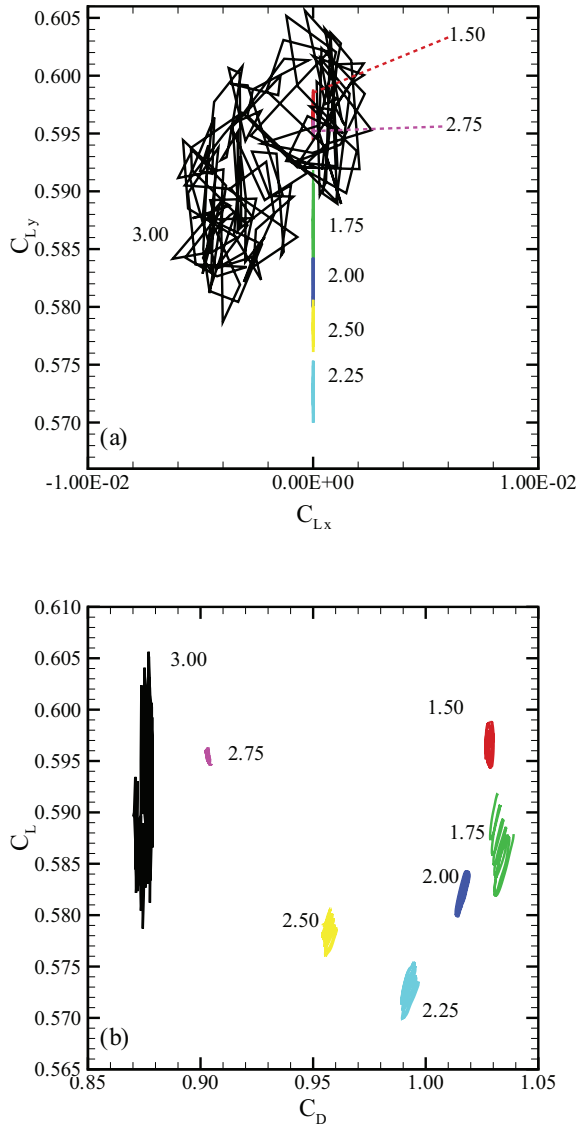


Figure 5: Phase diagrams for a transversely rotating sphere: (a)  $(C_{Ly}, C_{Lx})$  and (b)  $(C_L, C_D)$ .

One of the distinguishing features of certain regimes identified

in this study is the fact that the flow within them is not planar symmetric. This was noted as a qualitative difference between certain regimes but in order to look more closely at this feature, it is desirable to consider the difference in quantitative terms. In order to do so, phase diagrams  $(C_{Ly}, C_{Lx})$  and  $(C_L, C_D)$  can be constructed which show the magnitude of the different forces the sphere experiences, as illustrated in figure 5.

In figure 5(a) the dynamic relationship between the force in x and y is investigated. As is suggested by the name, the 'planar symmetric shear layer instability' regime has no component of force in the x-direction and hence the phase curve at  $\Omega^* = 1.50$  appears as a vertical line lying along axis  $C_{Lx} = 0$ . The length of this line along the  $C_{Ly}$ -axis indicates the amplitude of oscillatory forces in lift signal.

Likewise the flows which lie within the 'double period planar shear layer instability' regime are represented by vertical lines on the phase diagram along  $C_{Lx} = 0$  as would be expected from a planar system. In an earlier section, it is mentioned that the flow enters the 'double period asymmetric shear layer instability' regime at  $\Omega^* = 2.00$  and 2.25. However, as evident in the phase diagram  $(C_{Ly}, C_{Lx})$ ,  $C_{Lx}$  remains 0 for this flow regime with  $C_{Ly}$  keeps oscillating up and down along  $C_{Ly}$ -axis. The reason for  $C_{Lx} = 0$  may be attributed to the small component of flow moving out-of-plane as highlighted by the red ellipse in figure 3. As the movement of the out-of-plane flow is relatively small and is roughly at 3 diameters downstream, its effect on the hydrodynamic force is insignificant and thus  $C_{Lx}$  remains 0.

The most interesting representation of forces is at  $\Omega^* = 3.00$  where there are considerable force components in both the x and y-directions. These forces change energetically and rapidly so that when the forces are plotted for small number of cycles the locus has a sharp 'jagged' appearance. Plotting the forces for a large number of cycles reveals a locus with a full circular appearance. Rapid, sometimes sharp changes in the force coefficients suggest that the total force behaviour is the result of a number of small out-of-sync flow events. The rapid change is a result of the shifting dominance of certain small scale eddies as explored in figure 4.

In figure 5(b) the dynamic relationship between the lift and drag forces is explored. Overall, behaviour is similar across all the different regimes types. The most interesting feature from this image is the variation in the mean drag force as the rotation rate is increased. There is a monotonic decrease in drag with increasing rotation rate and the magnitude of the change is significant; a total change of around 0.18 across the range of rotations. Inspection of the pressure distribution around the sphere shows that this change in drag force is due to shifting pressure distributions at the rear of the sphere. As rotation rate is increased, the low pressure wake becomes gradually more deflected in the negative y-direction due to the momentum imparted on the flow at the sphere surface. The pressure at the region directly behind the sphere therefore gradually recovers, leading to decrease in the pressure drag. Viscous drag changes by only a small amount and hence the total drag is decreased.

### Strouhal Number

In figure 6 the Strouhal number,  $St = fd/U_\infty$ , is plotted against the non-dimensional rotation rate, where  $f$  is frequency of vortex formation calculated from the power spectrum of  $C_{Ly}$ . As would be expected from the preceding discussion, the frequency of vortex formation approximately halves as the regime shifts from simple 'shear layer instability' to the 'double period shear layer instability' regime. This is shown by an approximate halving of the Strouhal number between the two rotations. From  $\Omega^* = 1.75$  through to  $\Omega^* = 2.75$  the frequency of vortex forma-

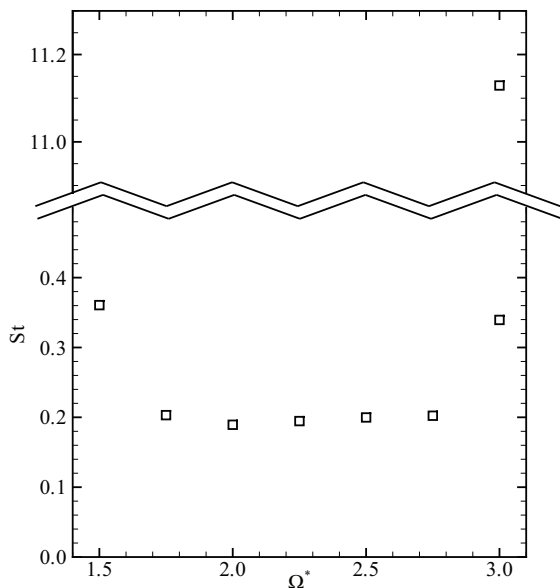


Figure 6: Strouhal number as a function of rotation rate (note discontinuous y-axis).

tion is approximately constant, resulting in a constant Strouhal number of approximately 0.22 across this range. At the rotation of  $\Omega^* = 3.00$  a power spectrum of the lift coefficient reveals two major frequency contributions to the signal, with one being much greater in frequency than the other. The lower frequency corresponds to the large scale vortex formation events which occur at a frequency comparable to the vortex formation of other rotation rates. The high frequency component is thought to correspond to the oscillations seen in the lift force as well as the transverse force in the  $x$ -direction and it is seen that these events occur mainly at a frequency which is approximately twenty-five times greater.

### Conclusions

In the present study, the flow of an incompressible fluid over a rotating sphere has been investigated numerically. Building on the results of co-workers, the study has focused on flows with a Reynolds number of  $Re = 300$  and non dimensional rotations in the range  $\Omega^* = 1.50$ – $3.00$ . It has been found that within this range of conditions, there are four different flow regimes that the fluid adopts depending on the rotation rate. For a rotation rate of  $\Omega^* = 1.50$  the flow is described as vortex formation via a ‘shear layer instability’ mechanism. As rotation rate is increased, a new flow regime develops at  $\Omega^* = 1.75$  which is termed in this paper the ‘double period planar shear layer instability’ regime. This flow regime is in many ways similar to the previous regime, with the exception that the frequency of vortex formation is now halved. This regime is noted to occur not only at a rotation of  $\Omega^* = 1.75$  but also at rotations of  $\Omega^* = 2.50$  and  $\Omega^* = 2.75$  and the vortices produced are planar and periodic in time. Bisecting this ‘double period’ regime is a flow condition known in this paper as the ‘double period asymmetric shear layer instability’ regime. Sharing many features in common with the flow type that surrounds it, the difference with this regime is the fact that the flow is no longer planar. In a flow with a sphere rotating at a rotation rate of  $\Omega^* = 3.00$  multiple flow phenomena are observed. Termed in this paper the ‘high frequency asymmetric shear layer instability’ regime, the flow under these conditions is highly energetic. A significant

transverse force in the  $x$ -direction exists which tends to oscillate the sphere sideways at a high frequency. The sphere also has an high frequency oscillation in the lift coefficient signal which enhances variation caused by large scale vortex formation events.

### References

- [1] Best, J.L., The influence of particle rotation on wake stability at particle Reynolds numbers,  $Re_p < 300$  – implications for turbulence modulations in two phase flows, *Int. J. Multiphase Flow*, **24**, 1998, 693–720.
- [2] Davis, A.M.J., Drag modifications for a sphere in a rotational motion at small, non-zero Reynolds and Taylor numbers: wake interference and possibly Coriolis, *J. Fluid Mech.*, **237**, 1992, 13–22
- [3] Giacobello, M., Ooi, A. and Balachandar. S., Wake structure of a transversely rotating sphere at moderate Reynolds numbers, *J. Fluid Mech.*, **621**, 2009, 103–130
- [4] Jeong, J. and Hussain, F., On the identification of a vortex, *J. Fluid Mech.*, **285**, 1995, 69–94
- [5] Johnson, T.A. and Patel, V.C., Flow past a sphere up to a Reynolds number of 300, *J. Fluid Mech.*, **378**, 1999, 378, 19–70
- [6] Kim, D., Laminar flow past a sphere rotating in the transverse direction, *J. Mech. Sci. Technol.*, **23**, 2009, 578–589
- [7] Loth, E., Lift of a solid spherical particle subject to vorticity and/or spin, *AIAA J.*, **4**, 2008, 801–809
- [8] Maccoll J.H., Aerodynamics of a spinning sphere, *J. Roy. Aero. Soc.*, **32**, 1928, 777–798
- [9] Newton I., New theory of light and color, *Phil. Trans. Roy. Soc.*, **1**, 1672, 678–688
- [10] Oesterlé, B and Dinh, B., Experiments on the lift of a spinning sphere in a range of intermediate Reynolds numbers, *Exp. Fluids*, **25**, 1998, 16–22
- [11] Poon E.K.W., Ooi, A.S.H., Giacobello, M. and Cohen, R.C.Z., Laminar flow structures from a rotating sphere: Effect of rotating axis angle, *Int. J. Heat Fluid Flow*, **31**, 2010, 961–972
- [12] Rubinow, S.I. and Keller, J.B., The transverse force on a spinning sphere moving in a viscous fluid, *J. Fluid Mech.*, **11**, 1961, 447–459
- [13] Tsuji, Y. Morikawa, Y. and Mizuno, O., Experimental measurement of the Magnus force on a rotating sphere at low Reynolds numbers, *Trans. ASME*, **107**, 1985, 484–488
- [14] Watts, R.G. and Ferrer, R., The lateral force on a spinning sphere: Aerodynamics of a curve ball, *Am. J. Phys.*, **55**, 1987, 40–44
- [15] You, C.F., Qi, H.Y. and Xu, X.C., Lift force on rotating sphere at low Reynolds numbers and high rotational speed, *Acta Mech. Sin. (Engl. Ser.) (China)*, **19**, 2003, 300–307